Enhanced thermoelectric properties of Sb2Te3/CH3NH3I hybrid thin films by post-annealing

Shuo Chen, Fu Li, Yuexing Chen, Jingting Luo, Guangxing Liang, Xianghua Zhang, Zhuanghao Zheng, Ping Fan

Journal Name

ARTICLE

Enhanced thermoelectric properties of Sb_2Te_3/CH_3NH_3I hybrid thin films by post-annealing

Received 00th January 20xx,
Accepted 00th January 20xx

DOI: 10.1039/x0xx00000x

Shuo Chen,[a] Fu Li,[a] Yuexing Chen,[a] Jingting Luo,[a] Guangxing Liang,[a] Xianghua Zhang, [b] Zhuanghao Zheng,*[,a] and Ping Fan[a]

In this work, to improve the *ZT* value of Sb_2Te_3, a novel concept of inorganic-organic hybridization is presented and the Sb_2Te_3/CH_3NH_3I hybrid thin films have been prepared via a post-annealing involved sequential sputtering/evaporating method. Results show that the crystallinity of the thin films are greatly improved after post-annealing and also with preferential orientations of (006) and (009) at appropriate temperature, leading to an obvious enhancement of electrical conductivity. Additionally, the hybrid thin films show uniform nano-sized grainy structures and the organic CH_3NH_3I has been successfully incorporated into the hybrid system in a stable state, thus resulting in the increase of Seebeck coefficient and decrease of thermal conductivity based on energy filtering effect. As expected, a maximum room-temperature *ZT* value of 0.56 for the Sb_2Te_3/CH_3NH_3I hybrid thin film annealed at 573 K can be obtained. This outcome further demonstrates a great potential for the inorganic-organic hybrid thin film in low temperature application scenarios.

Introduction

Thermoelectric (TE) materials can directly convert heat energy to electricity and have great potential applications in semiconductor cooling and power generator fields.[1] The development of TE generators for small electronic devices as the self-powered components has drawn tremendous research attentions due to its continuous power supply by using heat from other devices.[2] However, conventional TE materials are relatively bulky and naturally brittle, thereby limiting the development of micro-TE devices. By contrast, thin film TE materials are lightweight and easily prepared on various types of substrates, offering the possibility for micro-sized TE devices with broad applications in bendable and miniature scenarios.[3-6] The efficiency of the TE generator is determined by the properties of its intrinsic materials, which is closely related to a dimensionless figure of merit, expressed as $ZT=S\sigma T/\kappa$, where S is the Seebeck coefficient, σ is the electrical conductivity, T is the absolute temperature and κ is thermal conductivity.[7] Thus, simultaneously modifying S, σ, and κ to obtain TE material with high *ZT* value is essential to realize the efficient conversion for widespread commercial TE device applications. Recently, a new concept of TE performance improvement involved with inorganic-organic thin film TE nanocomposite materials has emerged. To be specific, combining the inorganic and organic components not only enhances the TE properties thanks to an energy filtering effect, but also extends the flexibility of inorganic materials.[8-11] For instance, Jin et al. fabricated Bi_2Te_3 thin film composites with highly ordered (0001)-textured nanocrystals on high-quality single-walled carbon nanotube (SWCNT) bundles by using sputtering method, demonstrating high *ZT* value and superior flexibility.[8] Zhang et al. prepared a p-type $Bi_{0.5}Sb_{1.5}Te_3$/PEDOT:PSS hybrid thin film that has over 2000% enhancement in the power factor.[9]

Classic antimony telluride-based thin films are well known as efficient thermoelectric materials that have been intensively studied and widely applied. For the thin film deposition, various techniques such as sputtering,[11-15] evaporation,[16]

[a] Shenzhen Key Laboratory of Advanced Thin Films and Applications, College of Physics and Optoelectronic Engineering, Shenzhen University, Shenzhen, 518060, China. Email: zhengzh@szu.edu.cn
[b] Univ Rennes, CNRS, ISCR (Institut des Sciences Chimiques de Rennes) UMR 6226, F-35000 Rennes, France

electron-deposition[17,18] and chemical vapor deposition[19] have been applied successfully. As aforementioned, the construction of an inorganic-organic hybrid framework can greatly enhance its pristine TE properties. An important organic material of CH_3NH_3I originated from inorganic-organic perovskite solar cells[20-23] was selected as the organic component in our previous work. Indeed, crystalline CH_3NH_3I-based materials have excellent electrical transport characteristic with carrier mobility as high as 10 $cm^2 V^{-1} S^{-1}$, which is beneficial for thermoelectric materials to obtain more superior thermoelectric properties. The Sb_2Te_3/CH_3NH_3I hybrid thin film prepared by using the multilayer deposition method has dramatically enhanced the Seebeck coefficient as well as a decrease of thermal conductivity, resulting in a significant increase of *ZT* compared with pure Sb_2Te_3 thin film.[24] However, the obtained TE properties are still somewhat unsatisfactory and obviously lower than those of the bulk antimony telluride-based materials. For example, Luo et al. reported a *ZT* value over 1.7 of Sb_2Te_3 could be obtained under high magnetic field,[25] and a value of 1.5 was also achieved after $FeTe_2$ doping as reported by Shin et al.[26] Therefore, improving its *ZT* value especially for the low temperature advantageous scenarios to broaden the scope of thin film based applications needs further exploration. In this work, the high-quality inorganic-organic Sb_2Te_3/CH_3NH_3I hybrid thin films were prepared by using magnetron sputtering combined with thermal evaporation method. The effect of post-annealing temperature on the TE properties was systematically investigated. As the result, a *ZT* value over 0.5 at room temperature of the hybrid thin film has been successfully obtained, surpassing the pure Sb_2Te_3 thin film and comparable with the maximum values of the Sb_2Te_3-based materials.

Experimental

Preparation of Sb_2Te_3/CH_3NH_3I hybrid thin films

At first, methylammonium iodide (CH_3NH_3I) and was synthesized by using methylamine (CH_3NH_2, Sigma Aldrich, 57 wt.% in H_2O) and hydroiodic acid (HI, Sigma Aldrich, 40 wt.% in H_2O) as raw materials. A mixture of 28 ml CH_3NH_2 and 30 ml HI was loaded into a 250 ml flask and stirred at 0 °C for 2 hours to form homogeneous precursor solution. Then it was transferred to a beaker and kept in a fixed temperature of 95 °C until obtaining the as-expected white CH_3NH_3I powder. The final purification process was carried out with diethyl ether for three times and the high-purity crystalline CH_3NH_3I powder can be obtained after drying at 60 °C in a vacuum chamber for 10 hours.

The Sb_2Te_3/CH_3NH_3I inorganic-organic hybrid thin films were prepared through a post-annealing involved sequential sputtering/evaporating method. A schematic illustration of the preparation process is shown in Fig. 1. Prior to deposition, the 1.5 mm BK7 glass was sequentially cleaned with acetone, alcohol, and deionized water for 15 min, and then dried under N_2 gas. The vacuum chamber was evacuated to an ultrahigh vacuum (2.0×10^{-4} Pa) prior to deposition. Initially, a high-purity Sb_2Te_3 (99.99%) sputtering target purchased from HZAM Co., Ltd was used, the Sb_2Te_3 layer was deposited onto the glass substrate with a thickness of approximately 200 nm by magnetron sputtering with a fixed power of 10 W. Then the CH_3NH_3I layer was evaporated onto the Sb_2Te_3 layer at a current of 100 A to a thickness of 100 nm. This evaporation process was carried out by a vacuum evaporating apparatus equipped in the same chamber and using the as-prepared CH_3NH_3I powder as source. Thereafter, another Sb_2Te_3 precursor layer was deposited onto the CH_3NH_3I layer to form a sandwich-structured inorganic-organic composite thin film. Finally, the thin films were post-annealed for 1 h under an Ar atmosphere with variable annealing temperatures.

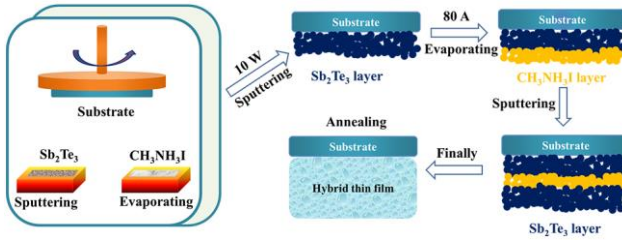

Fig. 1 Schematic illustration of the Sb_2Te_3/CH_3NH_3I hybrid thin films preparation process.

Characterization

The crystal structure of the thin films was investigated through X-ray diffraction (XRD, D/max2500, Rigaku Corporation) with Cu/Kα radiation at a voltage of 40 kV and a counting duration

of 10°/min ranging from 10° to 70°. Morphologies and elemental composition of the Sb_2Te_3/CH_3NH_3I hybrid thin films were obtained from a Zeiss supra 55 thermal field emission scanning electron microscope (SEM) equipped with an EDAX instrument. The room-temperature Raman scattering measurements were performed using a Lab Ram XploRA spectra system (Horiba Jobin Yvon). A steady-state spectrometer (Zolix Scan) equipped with a 325 nm HeCd laser as the excitation source was used to obtain photoluminescence (PL) spectra. The chemical valence was determined by conducting X-ray photoelectron spectroscopy (XPS, ESCALAB 250Xi) with a monochromatic Al Ka X-ray source of 1486.6 eV. The electrical conductivity and the Seebeck coefficient were simultaneously measured at room temperature by the Potential-Seebeck-Microprobe (PSM, Quantum Design) with a considered 7% instrument error. The carrier concentration and the Hall mobility were characterized using a Hall-effect measurement system (HL5500PC, Nanometrics) with Van der Pauw configuration at room temperature. The thermal conductivity at room temperature was determined by a transient hot-wire theory method (TC3000, Xiaxi Electronic Technology). To obtain the reliable value, each sample was measured for ten times and average value was used also with an estimated error of approximately 10%.

Results and discussion

Fig. 2 shows the XRD patterns of the as-prepared Sb_2Te_3/CH_3NH_3I hybrid thin films with different post-annealing temperatures. The diffraction peaks belonging to sample S1 annealed at 423 K present large full-width half maximum and low intensities, suggesting its poor crystallinity under this lower temperature circumstance. Then temperature-induced thin film crystallinity improvement can be observed also with a preferential orientation of (006) and (009). When the post-annealing temperature reached up to 573 K, all the sharp and prominent peaks are in agreement with the JCPDS standard card (71-0393) of the hexagonal phase of Sb_2Te_3 without any detectable impurity. The absence of an observable second phase of CH_3NH_3I is probably due to its low content.

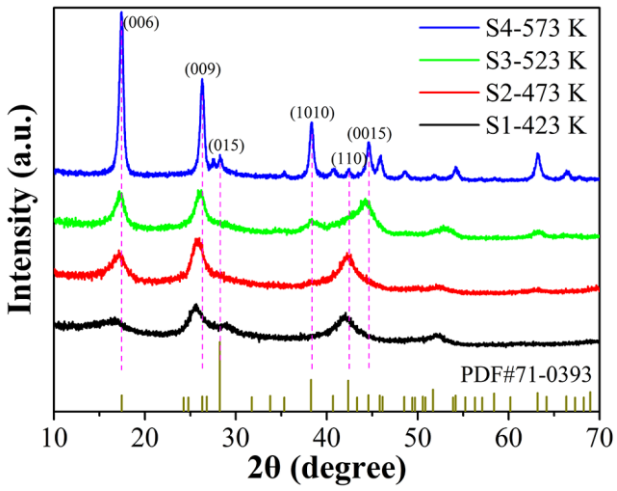

Fig. 2 XRD patterns of the Sb_2Te_3/CH_3NH_3I hybrid thin films.

To further investigate the crystalline nature and also the interior structures of the Sb_2Te_3/CH_3NH_3I hybrid thin films, Raman analysis has been carried out using a 514.5 nm laser in the range from 50 cm^{-1} to 300 cm^{-1}. As shown in Fig. 3a, no obvious peaks can be observed for sample S1, indicating its poor crystallization, which is consistent with the XRD results. With increasing the post-annealing temperature, some distinct peaks start to emerge and strengthen due to the improvement of thin film crystallinity. According to the theoretical calculations and previous experimental results, three major peaks located at 63, 106, and 159 cm^{-1} can match well with the A_{g1}, E_{g2}, and A_{g2} vibration modes of the Sb_2Te_3, respectively.[27] A slightly right shift of E_{g2} for the sample S4 is closely related to the incorporation of CH_3NH_3I after a high temperature post-annealing. Moreover, an additional peak at 133 cm^{-1} can be

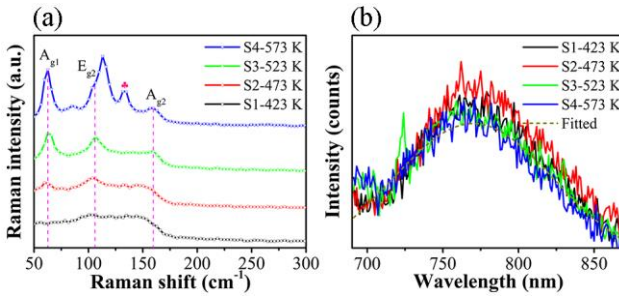

Fig. 3 (a) Raman scattering spectra and (b) photoluminescence spectra of the hybrid thin films obtained at room temperature.

identified as the vibration mode of the CH_3NH_3I based perovskite tetragonal crystal structure,[27,28] implying the existence of this second phase. Photoluminescence spectra is also an effective tool for organic component characterization, Fig. 3b shows the corresponding results of the hybrid thin films, one observable broad peak located at ~770 nm belonging to CH_3NH_3I further confirming that the as-prepared thin film consists of inorganic-organic hybrid structures.[29]

Fig. 4 presents the SEM images of the thin films, where temperature-induced surface morphology evolution has been clarified. A number of large clusters randomly dispersed on the surface can be observed for sample S1 (Fig. 4a), indicating the organic components have not been fully incorporated and exposed to a low post-annealing temperature. Significant decomposition and diffusion of these clusters occurred with an increase in the annealing temperature, leading to uniform nano-sized grainy structures in the thin film. Importantly, the as-designed sandwich-structure with CH_3NH_3I layer embedded in the middle position is really beneficial for this diffusion under post-annealing treatment. Further increasing the temperature to 573 K, as shown in Fig. 4d, sample S4 exhibits cocked plate-shaped features, implying the Sb_2Te_3/CH_3NH_3I hybrid thin film has a preferential growth direction that is perpendicular to the substrate, which is also consistent with the XRD results with (006) and (009) preferential orientation. Moreover, the dense and shaped plates with an average size of ~200 nm can benefit the charge transport properties and provide additional scattering centers to the propagation of phonons, thus resulting in a reduced thermal conductivity and also an increased Seebeck coefficient. The representative I content belonging to organic component of CH_3NH_3I has also been obtained from SEM-coupled EDS analysis, a slight decrease of atomic percent from 1.90% to 1.50% with increasing the post-annealing temperature further indicating it is essential to control the temperature.

XPS analysis was further conducted to investigate the valence states of the representative three constitute elements of Sb, Te and I. The corresponding high-resolution core level spectra obtained from all the hybrid thin films are shown in Fig. 5. A sharp peak located at 768.5 eV associated with Sb $3p_{3/2}$ is depicted in Fig. 5a, and no obvious modification can be observed with increasing the post-annealing temperature. Additionally, a high-resolution scan of Te 3d region (Fig. 5b) shows peaks at about 572.6 eV and 583.1 eV, which effectively match the reported values for the binding energies of Te $3d_{5/2}$ and Te $3d_{3/2}$ of Bi_2Te_3, respectively.[27] The other two peaks that synchronously exist toward higher binding energies at approximately 576.3 eV and 586.7 eV indicate the existence of oxidized states (Te^{4+}) on the surface, which is reasonable to occur after post-annealing of this composite thin film.[30] Finally, the spin orbit-coupled doublet of the I 3d core levels of all the thin films are split into $3d_{5/2}$ (~618.7 eV) and $3d_{3/2}$ (~630.2 eV) with a separation binding energy value of 11.5 eV,

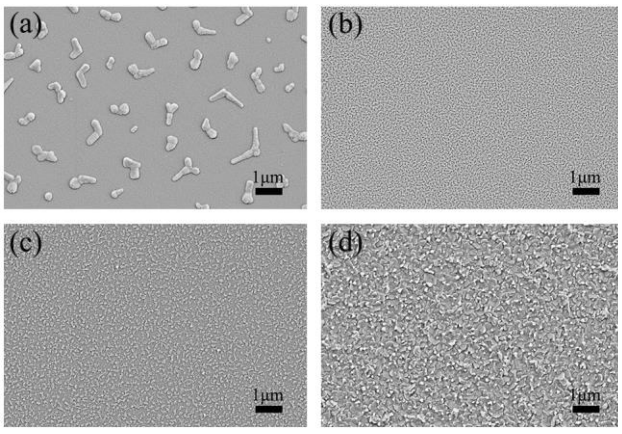

Fig. 4 SEM images of the Sb_2Te_3/CH_3NH_3I hybrid thin films.

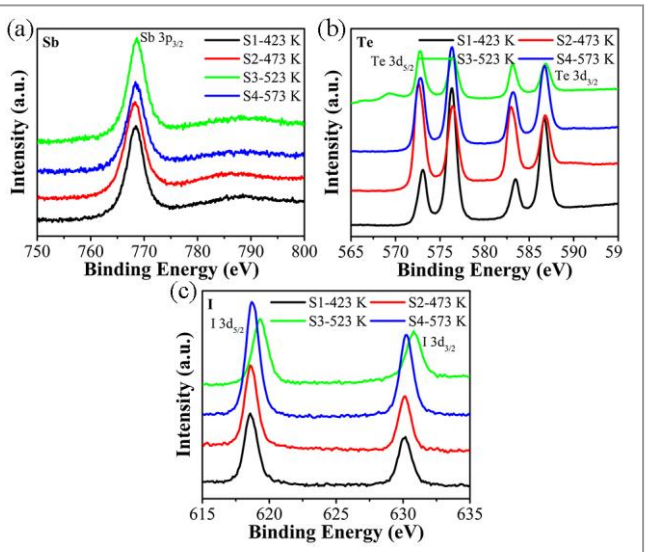

Fig. 5 XPS spectra of (a) Sb 3p, (b) Te 3d and (c) I 3d for the Sb_2Te_3/CH_3NH_3I hybrid thin films.

which is the typical peak position and separation of the spin-orbit components for I^-, further confirming that the organic CH_3NH_3I has been incorporated into the hybrid system in a stable state.

In the subsequent study, for a better comparison, the pure Sb_2Te_3 thin films with the same annealing treatment procedures have been prepared and denoted as P1, P2, P3 and P4, respectively. The Hall carrier concentration (n) and Hall carrier mobility (μ) of the pure Sb_2Te_3 thin films as well as the Sb_2Te_3/CH_3NH_3I hybrid thin films have been experimentally determined at room temperature and illustrated in Fig. 6. As shown in Fig. 6a, the pure Sb_2Te_3 thin film post-annealed at 423 K (sample P1) has a carrier concentration n as high as 9.91×10^{20} cm^{-3}, which is comparable to that of the reported bulk materials. As the post-annealing temperature increases, a significant linear decrease of n value can be observed, and it is closely related to the reduction of defect numbers after a more complete crystallization at high temperature. The temperature-induced grain growth and structure densification also lead to reduce the scattering of free electrons and therefore increasing the carrier mobility. This phenomenon resulted in a remarkable increase of carrier mobility μ from 0.08 $cm^2\ V^{-1}\ S^{-1}$ at 423 K to 11.3 $cm^2\ V^{-1}\ S^{-1}$ at 573 K for the pure Sb_2Te_3 thin films. Importantly, for the Sb_2Te_3/CH_3NH_3I hybrid thin films, an obvious decrease of Hall carrier concentration can be attributed to an enhanced scattering effect with adding the organic components as scattering centers. Meanwhile, the intrinsic n-type characteristic of CH_3NH_3I can also cause the recombination of partial electrons and holes, thus further reducing the carrier concentration of the hybrid thin film. Temperature-induced carrier mobility increase thanks to the improved crystallinity has also been observed in the hybrid thin films. Specifically, the μ values also show an increase of about 2-4 times compared with those of the pure Sb_2Te_3 thin films, and it is closely related to the formation of denser nanostructures in the existence of organic CH_3NH_3I. The enhanced carrier mobility (up to 44.4 $cm^2\ V^{-1}\ S^{-1}$) yields to a longer recombination life-time for carriers, which is undoubtedly beneficial for the migration of the electron/hole.

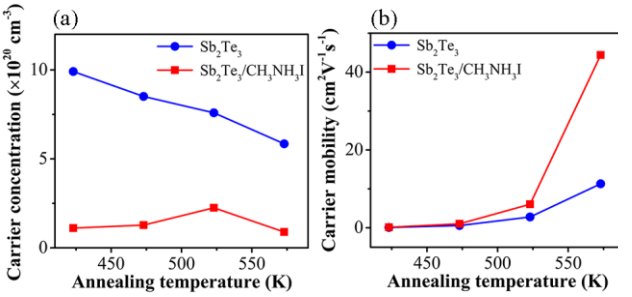

Fig. 6 Hall-effect measurements for the pure Sb_2Te_3 thin films and the Sb_2Te_3/CH_3NH_3I hybrid thin films: (a) Hall carrier concentration and (b) Hall carrier mobility.

Fig. 7 shows the room temperature thermoelectric properties of all the pure Sb_2Te_3 thin films and the Sb_2Te_3/CH_3NH_3I hybrid thin films. The corresponding values with attached error bars are determined by the measuring values with considered instrument errors and measuring errors. Fig. 7a presents the experimentally determined electrical conductivity σ of all the samples. A similar positive relationship between σ and post-annealing temperature can be observed for both pure Sb_2Te_3 thin films and Sb_2Te_3/CH_3NH_3I hybrid thin films. According to the typical expression of $\sigma=ne\mu$, where n is the carrier concentration, μ is the carrier mobility and e is the unit charge.[31] Thus, the carrier mobility is the dominant factor that accounts for the increase of electrical conductivity in the presence of a decreased carrier concentration as depicted previously. Moreover, the maximum σ values are 4.25×10^4 S m^{-1} and 3.1×10^4 S m^{-1} for the Sb_2Te_3 thin film and Sb_2Te_3/CH_3NH_3I hybrid thin film post-annealed at 573 K, respectively. This slight decrease is mainly caused by the decreased n value after incorporating the organic component, which cannot be fully compensated by the enhanced μ value. The Seebeck coefficients S of the thin films remain positive at those four different annealing temperatures, indicating their P-type nature, even after the incorporation of organic component (Fig. 7b). A normal quasi-linear positive relationship between the S values and the post-annealing temperatures for pure Sb_2Te_3 thin films can be explained by the reduction of some ionized impurities and improvement of crystallinity with increasing temperature. By contrast, the S values are obviously increased after the incorporation of CH_3NH_3I and reach a maximum value of 432.6 μV K^{-1} at 473 K

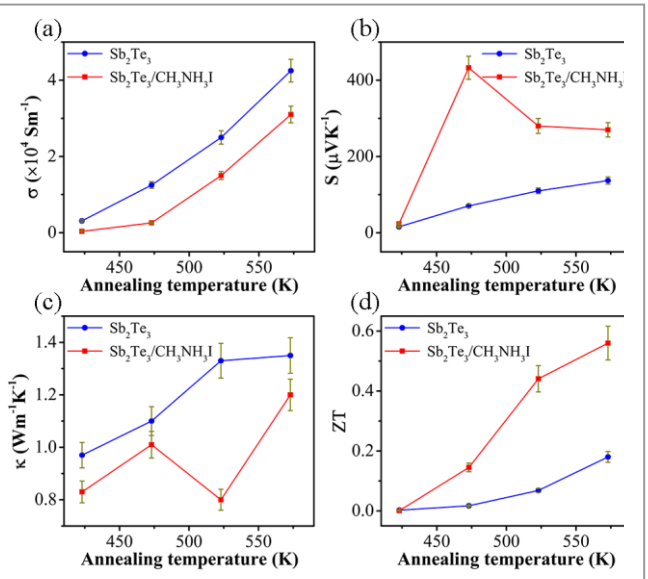

Fig. 7 (a) Electrical conductivity, (b) seebeck coefficient, (c) thermal conductivity and (d) *ZT* values of the pure Sb_2Te_3 thin films and the Sb_2Te_3/CH_3NH_3I hybrid thin films measured at room temperature.

for the Sb_2Te_3/CH_3NH_3I hybrid thin film. This improvement of *S* should be partially results from the reduced carrier concentration based on the Pisarenko relation.[32] Additionally, the band bending at the interfaces between the inorganic-organic inclusions can produce a significant scattering effect that might preferentially scatter low energy charge carriers, which can also enhance density of states and effective mass of carriers, thus are beneficial to the increase of *S* values.

The total thermal conductivity *k* measured at room temperature is shown in Fig. 7c. The *k* value of the pure Sb_2Te_3 thin film post-annealed at 423 K (sample P1) is 0.97 Wm^{-1} K^{-1}, which is lower than that of the bulk Sb_2Te_3 owing to its poor crystallinity. With increasing the post-annealing temperature, a significant increase of *k* value can be observed and it could inevitably diminish the improvement of final *ZT* value. By contrast, all the Sb_2Te_3/CH_3NH_3I hybrid thin films have a lower *k* value, especially an interesting value as low as 0.8 W m^{-1} K^{-1} for the highly crystalline inorganic-organic hybrid thin film post-annealed at 523 K (sample S3). Explanatorily, after the incorporation of organic CH_3NH_3I, it can scatter more phonons thanks to the existence of organic particles and defects. Moreover, the added abundant nanoscale or mesoscale boundaries between the inorganic and organic structures will further increase the effective scattering of phonons. Overall, this hybrid structure induced thermal conductivity decrease will undoubtedly beneficial for the improvement of *ZT* value. As shown in Fig. 7d, the calculated *ZT* values can be increased up to 8.5 times, 6.5 times and 3.1 times when comparing the hybrid thin films and the pure Sb_2Te_3 thin films with annealing treatment at 473 K, 523 K and 573 K, respectively. Notably, a maximum *ZT* value of 0.56 at room temperature for the Sb_2Te_3/CH_3NH_3I hybrid thin film is comparable with the maximum values of the Sb_2Te_3-based thermoelectric materials.[19,21] Furthermore, a *ZT* value of 0.15 for the Sb_2Te_3/CH_3NH_3I hybrid thin film annealed at 473 K is comparable with 0.18 for the pure Sb_2Te_3 thin film annealed at 573 K. This obvious 100 K net further demonstrates a great potential for the inorganic-organic hybrid thin film in low temperature application scenarios.

Conclusions

In summary, an effective magnetron sputtering combined with thermal evaporation method has been used to prepare the inorganic-organic Sb_2Te_3/CH_3NH_3I hybrid thermoelectric thin films. The post-annealing process induced crystallization, surface morphology evolution as well as the construction of a stable hybrid framework of the thin films can be observed. Moreover, with increasing the annealing temperature, the Sb_2Te_3/CH_3NH_3I hybrid thin films exhibit an obvious improvement in electrical conductivity and Seebeck coefficient. Thanks to its effective scattering of phonons in the hybrid structure, a decrease of thermal conductivity is also beneficial for the TE performance improvement. As a result, a *ZT* value as high as 0.56 at room temperature for the Sb_2Te_3/CH_3NH_3I hybrid thin film has been successfully obtained, which is totally surpassing the pure Sb_2Te_3 thin film and is comparable with the maximum values of the Sb_2Te_3-based thermoelectric materials, further demonstrating its great application potential in low temperature scenarios.

Conflicts of interest

There are no conflicts to declare.

Acknowledgements

This work is supported by National Natural Science Foundation of China (No. 11604212), Shenzhen Key Lab Fund (ZDSYS 20170228105421966), and Natural Science Foundation of SZU (grant No. 85304/00000297).

Notes and references

1 P. J. He and T.M. Tritt, *Science*, 2017, **357,** 1369.
2 Y. Wang, L. Yang, X. L. Shi, X. Shi, L. D. Chen, M. S. Dargusch, J, Z. Zhi and G. Chen, *Adv. Mater.* 2019, **31,** 1807916.
3 Z. Y. Lu, M. Layani, X. X. Zhao, L. P. Tan, T. Sun, S. F. Fan, Q. Y. Yan, S. Magdassi and H. H. Hng, *Small*, 2014, **10,** 3551.
4 A. L. Hansen, T. Dankwort, M. Winkler, J. Ditto, D. C. Johnson, J. D. Koenig, K. Bartholomé, L. Kienle and W. Bensch, *Chem. Mater.* 2014, **26,** 6518.
5 X. Mu, H. Zhou, D. He, W. Zhao, P. Wei, W. Zhu, X. Nie, H. Liu and Q. Zhang, *Nano Energy*, 2017, **33,** 55.
6 W. Zhu, Y. Deng and L. Cao, *Nano Energy*, 2017, **34,** 463.
7 C. Zhang, X. A. Fan, J. Hu, C. Jiang, Q. Xiang, G. Li, Y. Li and Z. He, *Adv. Eng. Mater.*, 2017, **19,** 1600696.
8 Q. Jin, S. Jiang, Y. Zhao, D. Wang, J. Qiu, D. M. Tang, J. Tan, D. M. Sun, P. X. Hou, X. Q. Chen, K. P. Tai, N. Gao, C. Liu, H. M. Cheng and X. Jiang, *Nat. Mater.*, 2019, **18,** 62.
9 T. Zhang, K. Li, C. Li, S. Ma, H. H. Hng and L. Wei, *Adv. Electron. Mater.*, 2017, **3,** 1770017.
10 H. Shi, C. Liu, Q. Jiang and J. Xu, *Adv. Electro. Mater.* 2015, **1,** 1500017.
11 F. Li, J. T. Luo, Z. H. Zheng, G. X. Liang, A. H. Zhong, Y. X. Chen and P. Fan, *J. Mater. Sci.*, 2019, **54,** 9565.
12 W. Y. Lee, N. W. Park, S. G. Yoon and S.K. Lee, *J. Nanosci. Nanotechno.*, 2016, **7,** 7567.
13 I. Hilmi, A. Lotnyk, J. W. Gerlach, P. Schumacher and B. Rauschenbach, *APL Mater.*, 2017, **5,** 050701.
14 V. D. Das, N. Soundararajan and M. Pattabi, *J. Mater. Sci.*, 1987, **10,** 3522.
15 N. Hatsuta, D. Takemori and M. Takashiri, *J. Alloys Compd.*, 2016, **685,** 147.
16 G. Bulman, P. Barletta, J. Lewis, N. Baldasaro, M. Manno, A. Bar-Cohen and B. Yang, *Nat. Commun.*, 2016, **7,** 10302.
17 Z. H. Zheng, P. Fan, J. T. Luo, G. X. Liang and D. P. Zhang, *J. Electron. Mater.*, 2013, **42,** 3421.
18 W. Jang, J. Lee, C. In, H. Choi and A. Soon, *ACS Appl. Mater. Interfaces*, 2017, **9,** 42050.
19 S. Shen, W. Zhu, Y. Deng, H. Zhao, Y. Peng and C. Wang, *Appl. Surf. Sci.*, 2017, **414,** 197.
20 C. Cho, B. Stevens, J. H. Hsu, R. Bureau, D. A. Hagen, O. Regev, C. Yu and J. C. Grunlan, *Adv. Mater.*, 2015, **19,** 2996.
21 H. Shi, C. Liu, J. Xu, H. Song, B. Lu, F. Jiang, W. Zhou, G. Zhang and Q. Jiang, *ACS Appl. Mater. Interfaces*, 2013, **5,** 12811.
22 L. Wang, X. Jia, D. Wang, G. Zhu and J. Li, *Synth. Met.*, 2013, **181,** 79.
23 S. N. Patel, A. M. Glaudell, D. Kiefer, and M. L. Chabinyc, *ACS Macro Lett.*, 2016, **5,** 268.
24 E. S. Kim, J. Y. Hwang, K. H. Lee, H. Ohta, Y. H. Lee and S. W. Kim, *Adv. Mater.*, 2017, **29,** 1604899.
25 Y. Luo, J. Yang, Q. Jiang, L. Fu, Y. Xiao, W. X. Li, D. Zhang, Z. Zhou and Y. Cheng, *Nano Energy*, 2015, **15,** 709.
26 W. H. Shin, O. W. Roh, B. Ryu, H. J. Chang, H. S. Kim, S. Lee, W. S. Seo and K. Ahn, *ACS Appl. Mater. Inter.* 2018, **104,** 3689.
27 Z. Zheng, P. Fan, J. Luo, G. Liang, H. Ma, X. Zhang, C. Yang and Y. Q. Fu, *Nanoscale*, **10**, 13511-13519.
28 B. Park, S. M. Jain, X. Zhang, A. Hagfeldt, G. Boschloo and T. Edvinsson, *ACS Nano*, 2015, **9,** 2088.
29 C. C. Stoumpos, C. D. Malliakas and M. G. Kanatzidis, *Inorg. Chem.*, 2013, **52,** 9019.
30 T. S. Su, Y. W. Yin, M. L. Teng, Z. Z. Gong, M. J. Zhang and X. G. Li, *J. Appl. Phys.*, **114,** 183901.
31 T. Zhu, Z. Xu, J, He, J. Shen, S. Zhu, L. Hu, T. M. Tritt and X. Zhao, *J. Mater. Chem. A*, 2013, **1,** 11589.
32 H. Wang, Z. M. Gibbs, Y. Takagiwa and G. J. Snyder, *Energy Environ. Sci.*, 2014, **7,** 804.